Spectroscopic study of intraminiband and interminiband tunneling in finite superlattices

J. W. Sleight
Department of Applied Physics, Yale University, P.O. Box 208284, New Haven, Connecticut 06520

R. J. Aggarwal
Department of Electrical Engineering, Massachusetts Institute of Technology, Cambridge, Massachusetts 02139

W. Duncan, Y.-C. Kao, and H. L. Tsai
Central Research Laboratories, Texas Instruments Incorporated, P.O. Box 655936, Mail Stop 136, Dallas, Texas 75265

W. R. Frensley and C. L. Fernando
Erik Jonsson School of Engineering and Computer Science, University of Texas at Dallas, Richardson, Texas 75083

M. A. Reed
Departments of Applied Physics and Electrical Engineering, Yale University, New Haven, Connecticut 06520
(Received 7 October 1994; revised manuscript received 23 January 1995)

We present a tunneling density-of-states study of transport between minibands in a series of $Ga_xAl_{1-x}As$ superlattice structures. We observe the eigenstates of the finite superlattice systems below the Stark localization threshold by tunneling spectroscopy. The tunneling spectroscopy agrees well with self-consistent Thomas-Fermi calculations. The eigenstate strengths are observed to thermally broaden as expected, and evidence for longitudinal-optical-phonon replicas of the eigenstate structure is presented.

I. INTRODUCTION

The artificial creation of periodic structures and superlattices, and the characterization of them using electron transport and optical techniques, has been a very active research area. In the $GaAs/Al_xGa_{1-x}As$ material system, varying the barrier and well thicknesses as well as the barrier heights gives great control over the created lattice, and therefore the type of band structure one can study. In weakly coupled superlattices it has been shown[1] that perpendicular transport proceeds via sequential tunneling, whereas under the proper conditions a miniband forms[2–4] possessing a constant two-dimensional (2D) density of states inside the band.

In the limit where there are few superlattice periods (N) and the miniband width (ΔW) is relatively wide, it is possible to experimentally probe the individual eigenstates which compose the miniband when $kT/(\Delta W/N) \ll 1$. Relatively little work has focused on this aspect of miniband formation, where the transport in the structure shifts from sequential tunneling through coupled quantum wells to coherent transport through minibands. Davies, Kelly, and Kerr[5] investigated a superlattice/barrier/superlattice structure. Under external bias, electrons are injected through a barrier from the Fermi level of one superlattice (hereafter defined as the emitter) into the downstream (collector) superlattice, allowing a study of the density of states of the collector superlattice. More recently,[6] work involving superlattice/barrier/superlattice structures (superlattice tunnel diode) has shown the existence of individual finite superlattice eigenstates. Here we present a tunneling density-of-states study of the transition from a superlattice miniband to a coupled-well structure for both interminiband and intraminiband cases, and evidence for intraminiband tunneling processes involving longitudinal-optical (LO)-phonon emission. The aim of this study is to investigate both the band structure of superlattices and the electron transport through superlattice minibands. The superlattices are characterized by photoluminescence and transmission electron microscopy, as well as electrical spectroscopy.

II. EXPERIMENT

Figure 1(a) is a self-consistent conduction band diagram at resonant bias. Figure 1(b) is a transmission electron micrograph (TEM) of the type of superlattice tunnel diode structure investigated in this study. This specific example is identical to the initial work of Davies, Kelly, and Kerr.[5] The band diagram is determined from a self-consistent finite temperature Thomas-Fermi zero-current calculation, and the quantum states are found by direct evaluation of the resonances of the effective-mass Hamiltonian.[7] Under voltage bias, the current will flow through the superlattice tunnel diode until the top of the first collector miniband crosses the bottom of the available emitter electron supply. Subsequently a decrease in the current occurs due to the requirement to conserve both energy and momentum.

This superlattice tunnel diode structure (consisting of a superlattice emitter, a relatively thick barrier, and a superlattice collector) is utilized to study the density of states of a series of superlattice structures. The barrier is

0163-1829/95/51(16)/10701(8)/$06.00

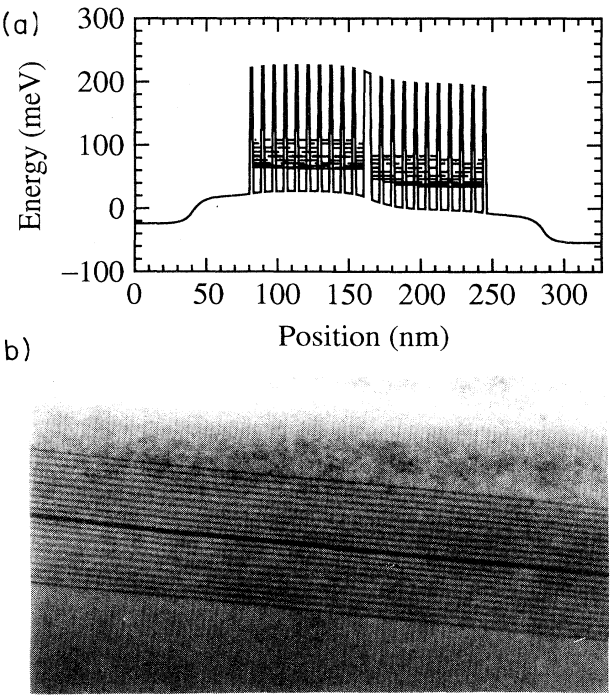

FIG. 1. (a) Self-consistent Γ-point conduction band vs the epitaxial dimension of sample 1 at resonant bias. The dotted lines denote the eigenstates that form the miniband. (b) A TEM (transmission electron micrograph) of sample 1. For scale, the dark wider central line (the tunnel barrier) is 55 Å.

used primarily to narrow the energy distribution of the electrons that tunnel into the collector. Table I illustrates the series of superlattice structures investigated. Superlattice dimensions are determined from TEM's, and the Fermi level and miniband positions are calculated using a fully self-consistent Poisson-Schrödinger calculation.[8] All structures were grown in a Riber 2300 MBE (molecular beam epitaxy) on In-free mounted GaAs wafers. Sample 1 was grown nominally identical to that of Davies, Kelly, and Kerr[5] in order to compare to previous work; however TEM reveals some differences in our structure (i.e., somewhat smaller barrier and wells widths than in the work of Davies, Kelly, and Kerr, although their TEM's revealed ±5-Å variances across the structure, as well as an asymmetry between the collector and emitter superlattices). The remaining samples consist of a Cr-doped semi-insulating GaAs substrate, a 0.5-μm undoped GaAs buffer, a 1-μm 1×10^{18}-cm^{-3} Si-doped n^+ GaAs bottom contact, a 420-Å 1×10^{17}-cm^{-3} (last 20 Å undoped) GaAs contact to superlattice transition region, a superlattice/tunnel barrier/superlattice region symmetric about the tunnel barrier, a 420-Å 1×10^{17}-cm^{-3} (first 20 Å undoped) GaAs contact to superlattice transition region, a 400-Å 2×10^{18}-cm^{-3} GaAs top contact, and an $In_xGa_{1-x}As$ top nonalloyed Ohmic contact. Samples 1, 2, 3, 4, 5, and 7 contain 10-period superlattices. The GaAs wells of these superlattices are doped at 1×10^{17} cm^{-3}, the barriers are nominally undoped, and the tunneling barrier is kept fixed at 88 Å (except for sample 7, which has a 167-Å barrier) of $Al_{0.23}Ga_{0.77}As$. To ensure accurate superlattice spectroscopy, the tunneling barrier must be the dominant impedance in the structure, and be sufficiently thick to decouple the 10-period superlattices on either side of the barrier. Sample 2 has the same approximate miniband width (33 meV) as sample 1, except the position of the miniband is higher (approximately by a factor of 2) in energy with respect to the conduction band of GaAs, making the second miniband completely virtual (i.e., the second miniband is entirely above the conduction-band edge, in bulk, of the superlattice barriers). Sample 3 is designed to have the same miniband centroid as sample 2, except with a miniband width five times larger (165 meV). In addition, it has symmetric 400-Å 1×10^{17}-cm^{-3} contact regions adjacent to the superlattices to study the effect of contacts. Sample 4 is designed to have a very large miniband width (214 meV, with the top 51 meV of the first miniband virtual with respect to the $Al_xGa_{1-x}As$ tunnel barrier), having easily experimentally resolvable eigenstates spaced by approximately 21 meV. Sample 5 is identical to sample 4, except that the bottom superlattice is replaced with bulk GaAs (though the doping modulation is identical), to investigate injection into a superlattice from a three-dimensional system, and vice versa. Sample 6 is identical to sample 5, except with a change in the number of superlattice periods from 10 to 20. Sample 7 explores the intraminiband tunneling regime by having three minibands: a very narrow (~9 meV) $n=1$ miniband, and much wider $n=2$ (44 meV) and 3 (74 meV) minibands.

For each superlattice structure designed for transport measurements, a photoluminescence control wafer and an

TABLE I. A summary of parameters for the seven superlattice samples. The first column lists the sample number. The second column lists the thickness of the well and barrier ($d_{GaAs}/d_{Al_xGa_{1-x}As}$), the third column lists the bottom of the superlattice minibands relative to the GaAs conduction band edge ($E_{n,SL}$-$E_{C,GaAs}$), the fourth column lists the miniband widths (ΔW), and the last column lists the Fermi level in the superlattice minibands relative to the GaAs conduction-band edge ($E_{F,SL}$-$E_{C,GaAs}$).

Sample	$d_{GaAs}/d_{Al_xGa_{1-x}As}$ (Å)	$E_{n,SL}$-$E_{C,GaAs}$ (meV)	Width (ΔW) (meV)	$E_{F,SL}$-$E_{C,GaAs}$ (meV)
1	52/21	45,204	44,199	47
2	34/42	87	33	87
3	41/10	35	165	46
4,5,6	36/9	37	214	47
7	117/25	19,77,176	9,44,74	27

electrical device wafer were grown. The photoluminescence structures consist of undoped superlattices clad in $Al_xGa_{1-x}As$. The photoluminescence of the nominally identical superlattices are used to verify the superlattice band gap. All photoluminescence measurements hereafter quoted are for the undoped superlattice control samples, not the transport samples. Devices are fabricated using contact lithography, lift-off metallization processes, a conventional alloyed Ni/Ge/Au composite bottom contact, and wet chemical etching to form various size mesa devices as small as 4 μm^2. A Si_3N_4/polyimide passivation layer is deposited over the entire structure prior to fabrication of vias and contacts to the individual devices. For all results presented, the positive bias will correspond to injection from the emitter (top contact), and the negative bias will correspond to injection from the collector (substrate side).

III. RESULTS

A. Narrow miniband samples

Sample 1 is a repeat of the structure of Davies, Kelly, and Kerr.[5] The superlattice wells are 52 Å in width, with the middle 17 Å doped n type to 4×10^{17} cm^{-3}. The superlattice barriers are 21 Å wide, and the tunneling barrier separating the two superlattices is 55 Å thick. We calculate that the first miniband lies 45 meV above the GaAs conduction-band edge and extends for an additional 44 meV. The second miniband ranges from 204 to 403 meV above the GaAs conduction-band edge, creating a minigap of 105 meV. The calculated superlattice Fermi level lies 10 meV above the first miniband edge. Low-temperature photoluminescence data show a superlattice band gap of 1.580 eV, compared to a calculated band gap of 1.578 eV.

Devices 4 μm^2 in size are used for characterization of sample 1. Our experimental zero-bias device resistance and contact resistance at liquid-helium temperatures are 5 kΩ and 31 Ω, respectively. Figure 2 shows the current-voltage (I-V) and conductance-voltage (G-V) characteristics of this structure at 4 and 300 K. We see a major low-voltage resonance at ±50 mV, with less evident resonances observable in the derivative at about ±400 and >500 mV. There are few changes in the characteristics from 10 to 100 K. From 100 to 300 K the valley current increases monotonically.

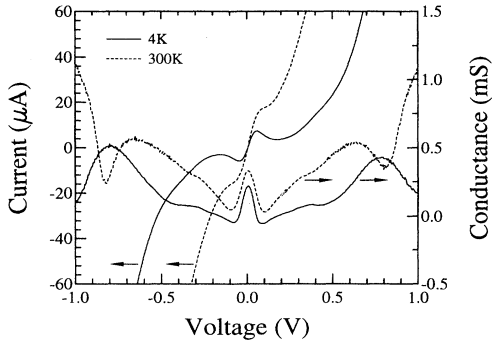

FIG. 2. Sample-1 current-voltage and conductance-voltage characteristics of a 4-μm^2 superlattice tunnel diode at $T=4$ and 300 K. Negative (positive) voltages correspond to injection from the surface (substrate) superlattice.

Our calculations show that the emitter and collector minibands no longer overlap at ±50 mV. For biases between the current peak and valley (50 mV < V < 150 mV), the emitter Fermi level is aligned with the first collector minigap. This indicates that the 50-mV resonance is the $n=1$ emitter to $n=1$ collector interminiband transition. Notice the finite zero-bias conductance due to the equilibrium lineup of these minibands. The higher-bias structure at about ±400 mV corresponds to the $n=1$ emitter to $n=2$ collector transition. This is in good agreement with the calculated value of 420 mV. The higher (>500 mV) structure is unidentified, being either injection into the indirect-band minima or Gunn effect.

There is little change in the low-voltage peak position with increasing temperature. However, the higher resonance shifts to lower bias, reflecting the increase of inelastic thermally generated background current. The low-bias ($n=1$ emitter miniband to $n=1$ collector miniband tunneling transition) conductance peak only shifts up by a constant conductance with increasing temperature, indicating that thermally generated inelastic tunneling is the dominant leakage current. Compared to Davies, Kelly, and Kerr,[5] the stronger 300-K resonant structure here implies that material parameters are important in determining the magnitude of thermally generated inelastic tunneling, in this case about 500 nS/K above 100 K.

We now investigate how these characteristics change as a function of the miniband position using sample 2, which has a miniband width similar to sample 1, and also has a virtual second miniband. Sample 2 is a 10-period, 34-Å well/42-Å barrier superlattice on either side of a 88-Å tunnel barrier. The superlattice has a thin bound miniband, 33 meV wide, located 87 meV above the GaAs conduction-band edge (versus 45 meV for sample 1). The second miniband, a virtual band, lies from 263 to 454 meV, which is above the $Al_xGa_{1-x}As$ conduction-band edge. The calculated Fermi energy of the superlattice at 4.2 K is ~2 meV above the lower edge of the first miniband. Low-temperature photoluminescence shows an experimental band gap of the superlattice of 1.622 eV, in excellent agreement with the calculated band gap of 1.622 eV.

Figure 3 shows the I-V and G-V data of the sample-2 superlattice tunnel diode structure at 173 and 300 K. At low temperature ($T<150$ K), the I-V is asymmetric in current, and the position of the $n=1$ emitter to $n=1$ collector resonance for both the positive and negative voltages shifts to lower biases with an increase in temperature. The asymmetry in I-V characteristics at low temperature can be explained by carrier freeze-out in the high resistance contacts (note the asymmetric epitaxial contact structure). Thus here we concentrate on higher-temperature data where this is not a contributing factor. Even at 173 K a slight asymmetry in the G-V around zero bias is observable. Variable-temperature measurements show a forward peak current maximum at 187 K, a reverse at 110 K, the maximum peak-to-valley current ratios of 1.62 for forward bias and 2.34 for reverse bias

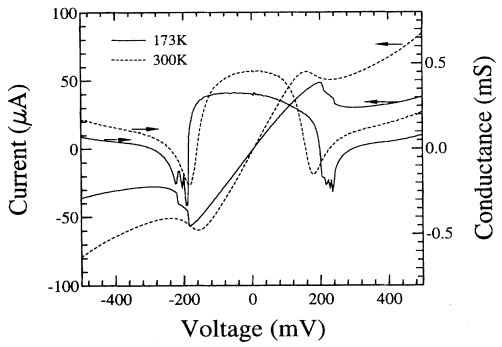

FIG. 3. Sample-2 current-voltage and conductance-voltage characteristics of a 9-μm^2 superlattice tunnel diode at $T=173$ and 300 K. Negative (positive) voltages correspond to injection from the surface (substrate) superlattice.

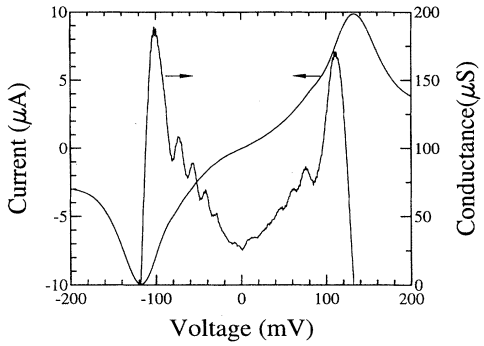

FIG. 4. Sample-3 current-voltage and conductance-voltage characteristics of a 9-μm^2 superlattice sample at $T=4.2$ K. Negative (positive) voltages correspond to injection from the surface (substrate) superlattice. Note the fine structure in the conductance trace, due to the collector superlattice eigenstates.

occurring at the same temperature that the current peak occurs. This implies that the peak-to-valley ratio is dominated, even at relatively high temperature, by the elastic tunneling current. The valley current dependence does not reveal an activated process. The major resonances of the device occur at $+196$ and -188 mV at $T=173$ K. Higher-bias data (>1 V) show little structure at any temperature.

Compared to sample 1, there is a dramatic increase in the strength of the $n=1$ tunneling resonance due to changing the position and width of the miniband. The 300-K *I-V* of sample 2 [with a peak-to-valley (P/V) current ratio of 1.3 at 300 K (2.4 at 4.2 K)] is quite similar to the 4.2-K *I-V* of sample 1 (P/V of 2). The peak conductance is ~ 100 μS higher in sample 1, consistent with a higher-energy miniband. Aside from the major resonances (with the exception of a weak LO-phonon emission shoulder present in sample 1, to be discussed below), there is no apparent additional structure in the conductance greater than the 1-mV experimental resolution for either sample 1 or sample 2 at a temperature of 4.2 K.

B. Medium/wide miniband sample

We now examine a single miniband sample with medium- and wide-range miniband width superlattices. In addition, contacts to the superlattices are altered to avoid the freeze-out effects seen in sample 2. Sample 3 is a structure with 41-Å superlattice wells and 10-Å superlattice barriers. The wells are doped n type to 1×10^{17} cm^{-3}. The structure has an 88-Å tunneling barrier. The first miniband of sample 3 is calculated to lie 35 meV above the conduction-band edge of GaAs, and extends for 165 meV. The second miniband ranges from 294 to 810 meV above the GaAs conduction-band edge. The calculated superlattice Fermi level lies 5 meV above the lower edge of the first superlattice miniband. Low-temperature photoluminescence shows an experimental superlattice band gap of 1.581 eV, compared to a calculated band gap of 1.575 eV.

Figure 4 shows the low-voltage *I-V* and *G-V* characteristics of sample 3 at 4.2 K. The $\pm\sim120$-mV major peak corresponds to the lineup of the first collector minigap with the emitter Fermi level. A series of peaks on the low-bias side of the major peak are apparent. Note that these biases correspond to electric fields well below that expected for Stark localization.[9,10] The condition for Stark localization of a superlattice is $eEd > \Delta W$, where E is the applied electric field, d is the superlattice period, and ΔW the width of the miniband under consideration. At the biases considered here, the Stark splitting is less than 10 meV, compared to a miniband width of 105 meV. The subresonant series starts to degrade above 20 K, and is unobservable (except for the highest subresonance peak) above 50 K.

The widest single miniband structure investigated (sample 4) has 36-Å well and a 9-Å barrier. The tunnel barrier of the structure is again 88 Å, and the superlattice wells were doped n-type to 1×10^{17} cm^{-3}. The first miniband in this structure is calculated to extend for 214 meV, from 37 to 251 meV above the GaAs conduction-band edge. The calculated superlattice Fermi energy lies in the first miniband, 55 meV above the GaAs conduction-band edge. Low-temperature photoluminescence gives an experimental band gap of 1.575 eV, compared to a calculated band gap of 1.578 eV.

Figure 5(a) shows the low-temperature *I-V* and *G-V* characteristics of a 9-μm^2 superlattice device. The major resonances of this device occur at $+432$ and -484 mV. In comparison to sample 3, this sample exhibits a more pronounced subresonance series, as can be viewed better in the conductance derivative [Fig. 5(b)]. The higher-bias peaks of this series are evident even at room temperature.

There are two possible explanations for the structure: Stark localization of the miniband, as previously discussed, or the existence of individual quantum states within the miniband. In the present case, the maximum Stark splitting would be ~30 meV, much lower than the miniband width of 214 meV. Thus the structure appears at too low a voltage to attribute the features to Stark localization of the miniband.

To determine if the structure is due to the finite extent of the superlattice, we calculate the single-electron

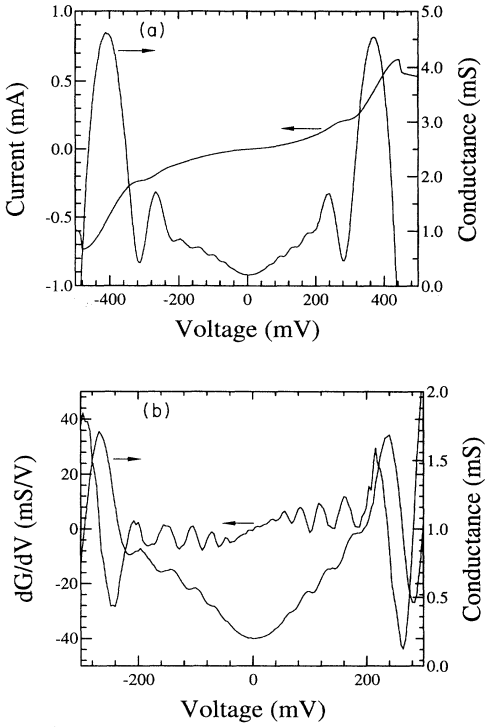

FIG. 5. (a) Sample-4 current-voltage and conductance-voltage characteristics at $T=4.2$ K. Negative (positive) voltages correspond to injection from the surface (substrate) superlattice. Note the fine structure in the conductance trace, due to the collector superlattice eigenstates. (b) Sample-4 conductance-voltage and derivative conductance-voltage characteristics for the same sample and conditions as in (a).

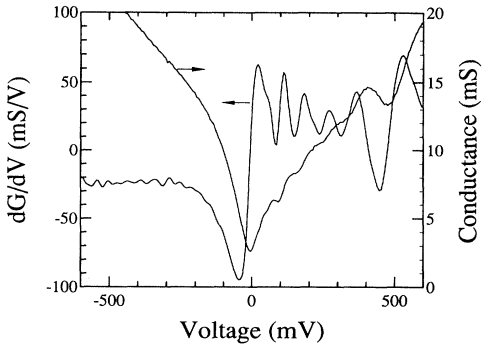

FIG. 7. Conductance-voltage and derivative conductance-voltage characteristics of sample 5 (the same as sample 4, except that one of the superlattices is replaced with bulk GaAs) at $T=10$ K. The positive bias corresponds to electron injection from the bulk GaAs into the finite superlattice. Note the absence of structure in the reverse bias.

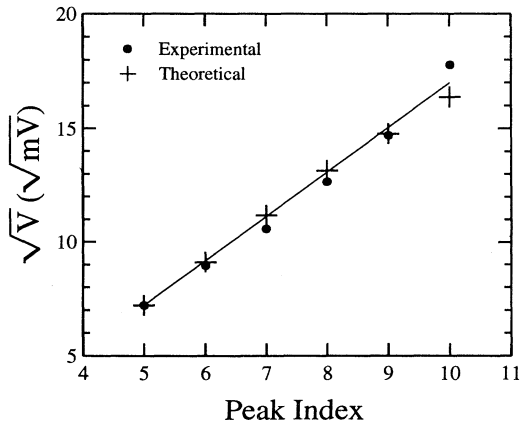

FIG. 6. Experimental (circle) and theoretical (cross) resonant crossings of the collector finite superlattice transmission peaks with the emitter superlattice Fermi level in sample 4. The calculated resonant crossings were determined from mapping the finite superlattice transmission peaks onto the self-consistent band structure, and determining the bias at which they cross the emitter Fermi level.

transmission coefficient of the 10-period superlattice and coupled-quantum-well system, and map these ten resonant peaks onto the self-consistent band structure. Figure 6 shows the calculated resonant crossings of the collector finite superlattice transmission peaks with the emitter Fermi level, compared with the experimental resonant peaks. The calibration of the top resonance is determined by the number of periods in the finite superlattice, and the low peak cutoff is determined from the superlattice Fermi level. The agreement between calculated and experimental peak positions is qualitatively (a $V^{1/2}$ behavior) and quantitatively good. High-voltage deviations may indicate that a zero-current model is no longer valid. Sample 4 provides an example of a superlattice whose number of periods is sufficiently small that effects of finite periodicity on the transmission coefficient can be seen in electron transport.

To check experimentally that the resonances are indeed arising from the collector density of states, we examine sample 5, which is identical to sample 4 but with

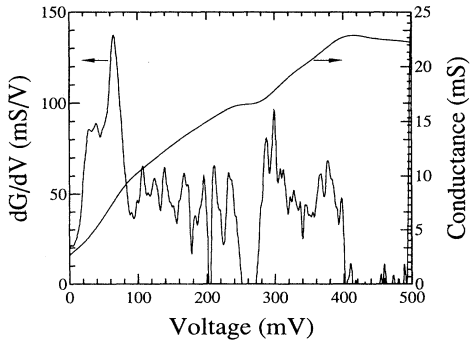

FIG. 8. Conductance-voltage and derivative conductance-voltage characteristics of sample 6 (sample 4 with 20 superlattice periods, instead of 10) at $T=4.2$ K.

bulk GaAs on one side of the superlattice.[11] Figure 7 shows the *G-V* characteristics of this structure at 10 K. Positive bias corresponds to electron injection from the bulk GaAs into the finite superlattice. Under this condition, the position and number of the subresonance peaks compare well with that of the finite superlattice injector sample. As has been pointed out earlier, there is no structure in the reverse-bias direction since the collector is bulk. It should be noted that the lower Fermi level in the bulk GaAs (versus the replaced superlattice) accounts for the voltage shift of the subresonant peaks.

Sample 6 is used as another check to assure that the collector density of states is the source of the resonances seen in both samples 4 and 5. As stated previously, this sample is identical to sample 4, except that the number of superlattice periods on either side of the tunnel barrier is now 20 instead of 10. To first order, this should double the number of resonances seen in the electron spectra, as now the miniband is composed of 20 eigenstates, compared to ten in sample 4. Seen in Fig. 8 is evidence of approximately 18 resonances from 0 to 400 mV, in reasonable agreement with the expected observable 18–19 states (since one or two are hidden below the collector Fermi level).

The absence of structure in samples 1 and 2, and the observation of structure in samples 3–6, implies that we have experimentally observed the transition from an indistinguishable miniband to a coupled-well structure. In energy, this implies that the transition occurs between state splittings of 3.7 (the maximum in sample 1) and 13.6 meV (the minimum observable in sample 3), when kT is less than the state splitting $E(\mathbf{i}+1)-E(\mathbf{i})$. Note that this is a function of the position of eigenstate **i** within the miniband. The origin of the eigenstate inhomogeneous broadening mechanism (such as epitaxial or alloy fluctuations) is not known.

C. Multiple miniband sample

In previous samples, transport in only one miniband was investigated. The last superlattice structure investigated is a multiminiband structure designed to show tunneling through a spectrum of higher-order minibands. In order to increase the number of minibands under the $Al_xGa_{1-x}As$ conduction-band edge, the superlattice well is widened. This structure has a 117-Å well and a 27-Å barrier. In order to compensate for the larger well, the resonant-tunneling barrier is increased to 167 Å. The calculated superlattice Fermi level lies 8 meV above the lower edge of the first miniband. The low-temperature photoluminescence of the control superlattice shows a superlattice band gap of 1.540 eV, compared to a calculated band gap of 1.533 eV.

Figure 9(a) shows a zero-bias Thomas-Fermi calculation[7] of the conduction-band edge and minibands at low temperature for sample 7. Three minibands are apparent. Using a more accurate fully self-consistent Poisson-Schrödinger calculation,[8] we calculate the positions of the minibands (referenced to the GaAs conduction-band edge) to be as follows: the first from 19 to 28 meV, the second from 77 to 111 meV, and the third from 176 to 250 meV. Figure 9(b) shows a calculation of the device under a bias of 120 mV. In this sample, the Fermi level is calculated to lie at 27 meV above the GaAs conduction-band edge, placing it near the top of the first, narrow (~9 meV wide) miniband; thus, injection occurs from the Fermi level near the top of the emitter miniband. In contrast to the preceding samples, in which all of the minibands were relatively wide, the narrowness of the first emitter miniband also contributes to the collimation of the electron energy distribution.

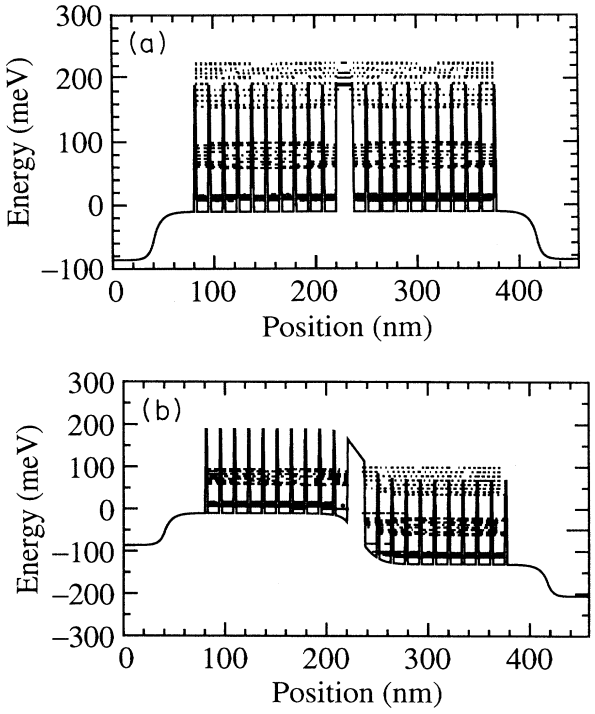

FIG. 9. (a) Self-consistent Γ-point conduction band vs the epitaxial dimension of sample 7 at zero bias. The dotted lines denote the eigenstates that form the three minibands. (b) Same as (a), with an applied bias of 120 mV. Note that the injection is now into the minigap between the collector $n=2$ and 3 minibands.

We expect the experimental spectroscopy to be more complex for sample 7, due to the multiple minibands. In order to better interpret the electron spectroscopy, a calculation similar to the procedure used in Fig. 6 is performed to examine the dependence of the collector superlattice density of states upon applied bias. The self-consistent Thomas-Fermi model is evaluated at several bias points to determine the conduction-band profile. Knowing the conduction-band profile, the eigenstate energies of the superlattice are calculated. Figure 10 shows how the eigenstate energies of the collector superlattice move with bias, with respect to the Fermi level in the emitter. When these states pass through the emitter Fermi level, an increase in conduction is expected due to the enhanced probability of tunneling into one of the collector superlattice eigenstates. Note how the topmost states of the $n=1$ and 2 collector minibands peel off due to Stark localization of the state near the depletion layer

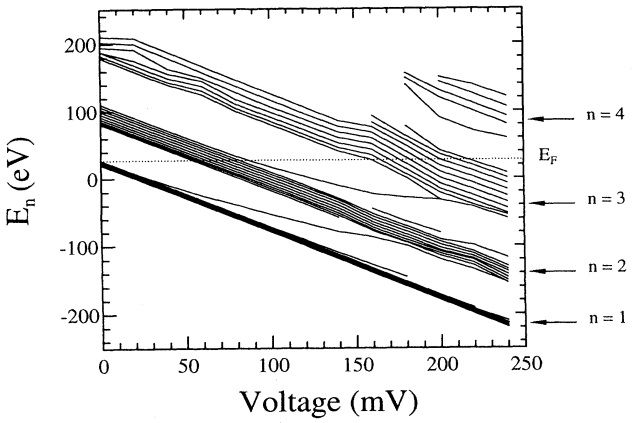

FIG. 10. Calculated collector superlattice eigenstate energies as a function of the applied voltage. Note how the top eigenstate in the $n=1$ and 2 minibands peel off and enter the $n=2$ and 3 minibands, respectively.

next to the barrier. As shown in Fig. 10, the Fermi-level crossings with the superlattice states occur for sample 7 in regimes where there are no peeled-off states, and thus are unfortunately not observable in this experiment. Observation of this previously unreported effect would require a different structure design. For the $n=1$ emitter to $n=1$ collector transitions, where ΔW is 9 meV, it would be possible to observe individual collector states for $T \ll 10.4$ K if the inhomogeneously broadened linewidth is less than 0.9 meV. For the $n=1$ emitter to $n=2$ collector and $n=1$ emitter to $n=3$ collector transitions, we expect that we should be able to resolve effects due to the individual eigenstates provided $T \ll 51$ K ($n=2$) or $T \ll 86$ K ($n=3$) *and* the inhomogeneously broadened linewidth is less than 4.4 ($n=2$) or 7.4 meV ($n=3$). Assuming that the origin of the inhomogeneous broadening is the same in this sample as in the previously discussed samples (e.g., nominally identical growth conditions), the previously determined inhomogeneous line broadening (between 3.7 and 13.6 meV) indicates that it will not be possible to resolve individual eigenstates in the $n=1$ miniband. Additionally, it will be difficult to observe individual eigenstates in the $n=2$ miniband, but it may be possible in the $n=3$ miniband.

Figure 11 shows the experimental current (dashed) and conductance (solid) versus voltage for sample 7. The conductance peak near 0 V is due to transport from the $n=1$ emitter miniband into the $n=1$ collector miniband. The conductance peak near 100 meV is due to transport into the $n=2$ collector miniband, and the peak near 200 meV is due to transport into the $n=3$ collector miniband. The position of the conductance peaks, and the valleys between them, agrees well with the calculated miniband positions (from Fig. 10) shown by the bars at the bottom of Fig. 11. Note that the small conductance rise at 0 mV, corresponding to the current peak at 10 mV, is caused by transport from the $n=1$ emitter into the $n=1$ collector. As discussed previously, the fine structure is not as clearly visible for sample 7 in the conductance traces.

Figure 12 shows two conductance derivative curves for sample 7, taken at two different temperatures, 1.4 (solid) and 16.5 K (dashed). Fine structure is observed in both of these traces. Nominally identical traces are obtained after thermally cycling the device to room temperature. Many traces taken at temperatures between 16.5 and 1.2 K show a gradual sharpening as temperature decreases, consistent with Fermi-level sharpening in the emitter. Although difficult to resolve due to the inhomogeneous broadening, the experimentally observed approximate peak separation for the $n=2$ and 3 transitions, $\Delta E(n=2) \sim 3.4$ meV and $\Delta E(n=3) \sim 8.5$ meV (using a energy/voltage conversion ratio of 0.85, determined from the band-structure modeling), is close to the theoretical

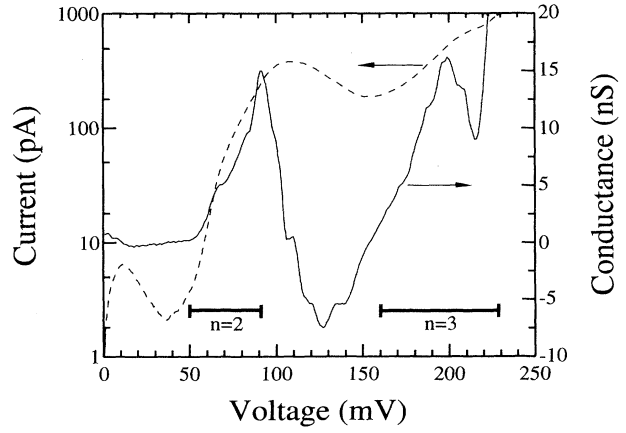

FIG. 11. Sample-7 current-voltage (dashed) and conductance-voltage (solid) characteristics of a 4-μm^2 superlattice sample at $T=4.2$ K. Positive voltages correspond to injection from the surface superlattice. Note the small fine structure in the conductance trace due to the collector superlattice eigenstates. Miniband positions determined from Fig. 10 are shown by the labeled bars.

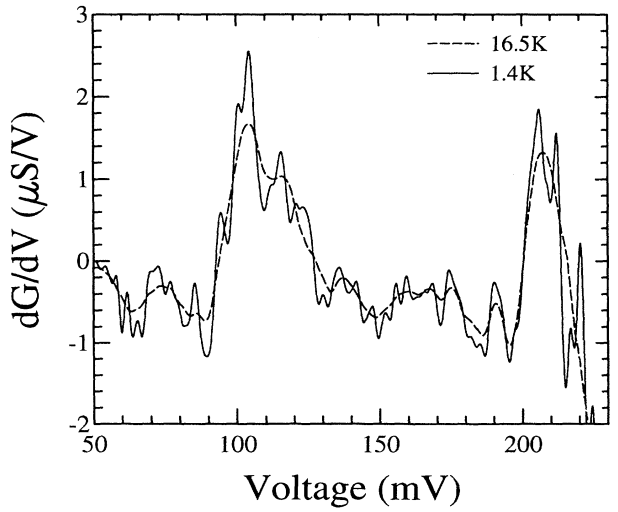

FIG. 12. Derivative conductance-voltage characteristics of sample 7 at $T=1.4$ (solid) and 16.5 K (dashed).

state separation of 4.4 meV for $n=2$ and 7.4 meV for $n=3$. Note that the observed inhomogeneous linewidths are $\gtrsim 3.4$ meV (as the $n=2$ states are barely resolvable), probably due to epitaxial structure imperfections and/or impurities. This implies that the $n=1$ states overlap, and is consistent with the inability to resolve them experimentally.

While some of this fine structure lies within the calculated $n=2$ and 3 minibands, note that additional peaks are observed between the calculated $n=2$ and 3 resonances. The similar temperature dependence of these additional peaks with those of the $n=2$ and 3 peaks suggests that these are also individual state peaks. A possible explanation for the additional peaks may be transitions involving a LO-phonon emission, which would span the entire $n=2$ to 3 minigap (i.e., $n=1 \rightarrow n=2+1$ LO). LO-phonon replicas, with a peak intensity of approximately five times less than the main resonance, are observable in these samples under appropriate conditions, e.g., for sample 1 near 90 mV in Fig. 2 if appropriately magnified (not shown). However, the strength of the additional peaks in sample 7 is larger than would be expected for LO-phonon replicas; thus the origin of the additional peaks is as yet not understood.

IV. CONCLUSIONS

We observe the transition in a GaAs/$Al_xGa_{1-x}As$ superlattice from a continuous narrow miniband to a larger miniband, where the finite period nature of the superlattice becomes important. We observe structure in tunneling spectroscopy for finite-period single and multiple miniband superlattice/barrier/superlattice samples that is attributed to the discrete eigenstates which form the miniband. Variable-temperature data show thermal broadening of the conductance structure due to changing the energy distribution of the electrons near the Fermi level in the emitter, as expected. The features in the conductance spectra are determined to arise from the collector density of states by both examining an asymmetric structure with no superlattice on one side of the barrier, and by varying the superlattice periodicity. The experimental electron spectroscopy results agree remarkably well with self-consistent Thomas-Fermi calculations.

ACKNOWLEDGMENTS

We thank A. Bouchard and J. Luscombe for superlattice calculations, M. Amman, C. Fonstad, E. S. Hornbeck, and M. J. Kelly for discussions, D. C. Collins and R. T. Bate for support, and R. K. Aldert, P. Q. Montague, E. D. Pijan, P. F. Stickney, F. H. Stovall, and J. R. Thomason for technical assistance. Portions of this work were done under the MIT-TI VI-A Internship Program, and was supported in part by the Office of Naval Research and a State of Connecticut Goodyear Grant.

[1] K. K. Choi, B. F. Levine, R. J. Malik, J. Walker, and C. G. Bethea, Phys. Rev. B **35**, 4172 (1987).

[2] T. Duffield, R. Bhat, M. Koza, F. DeRosa, D. M. Hwang, P. Grabbe, and S. J. Allen, Jr., Phys. Rev. Lett. **56**, 2724 (1986).

[3] B. Deveaud, J. Shah, T. C. Damen, B. Lambert, and A. Regreny, Phys. Rev. Lett. **58**, 2582 (1987).

[4] A. Sibille, J. F. Palmier, H. Wang, and F. Mollot, Phys. Rev. Lett. **64**, 52 (1990).

[5] R. A. Davies, M. J. Kelly, and T. M. Kerr, Phys. Rev. Lett. **55**, 1114 (1985).

[6] R. J. Aggarwal, M. A. Reed, W. R. Frensley, Y.-C. Kao, and J. H. Luscombe, Appl. Phys. Lett. **57**, 707 (1990).

[7] W. R. Frensley, Superlatt. Microstruct. **11**, 347 (1992).

[8] J. H. Luscombe, A. M. Bouchard, and M. Luban, Phys. Rev. B **46**, 10 262 (1992).

[9] R. F. Kazarinov and R. A. Suris, Fiz. Tekh. Poluprovodn. **5**, 797 (1971) [Sov. Phys. Semicond. **5**, 707 (1971)].

[10] L. L. Chang, L. Esaki, A. Segmüller, and R. Tsu, in *Proceedings of the Twelfth International Conference on the Physics of Semiconductors,* edited by M. H. Pilkuhn (Teubner, Stuttgart, 1974), p. 688.

[11] P. England, J. R. Hayes, J. P. Harbison, D. M. Hwang, and L. T. Florez, Appl. Phys. Lett. **53**, 391 (1988).

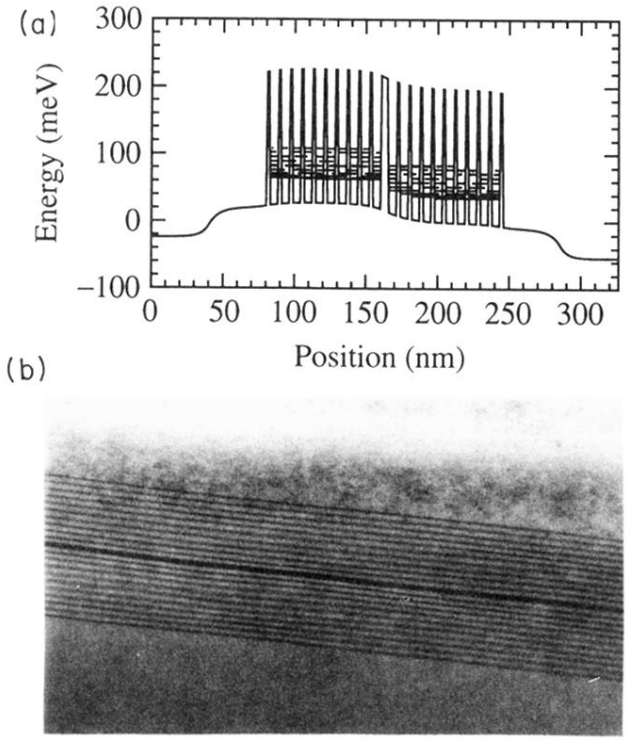

FIG. 1. (a) Self-consistent Γ-point conduction band vs the epitaxial dimension of sample 1 at resonant bias. The dotted lines denote the eigenstates that form the miniband. (b) A TEM (transmission electron micrograph) of sample 1. For scale, the dark wider central line (the tunnel barrier) is 55 Å.